

Influence of nanoparticle height on plasmonic resonance wavelength and electromagnetic field enhancement in two-dimensional arrays

John Henson, Jeff DiMaria, and Roberto Paiella^{a)}

Department of Electrical and Computer Engineering and Photonics Center, Boston University, 8 St. Mary's Street, Boston, Massachusetts 02215, USA

(Received 14 August 2009; accepted 29 September 2009; published online 13 November 2009)

A detailed experimental and theoretical study of the plasmonic properties of silver nanoparticle arrays as a function of nanoparticle height is presented. Specifically, several square periodic arrays have been fabricated by electron beam lithography and characterized via transmission spectroscopy measurements. The same arrays have also been numerically investigated via finite-difference time-domain calculations of their scattering and absorption cross sections and steady-state field intensity distributions. The results of this study show that the collective plasmonic resonances of these arrays can be effectively blueshifted by increasing the nanoparticle height, while at the same time maximizing the average field enhancement in the substrate and maintaining small absorption losses. This approach can therefore be used to extend the spectral reach of lithographically defined metallic nanoparticle arrays for practical applications such as light-emission efficiency enhancement. © 2009 American Institute of Physics. [doi:10.1063/1.3255979]

I. INTRODUCTION

Noble-metal individual nanoparticles (NPs) and NP arrays have been the subject of extensive study in recent years, due to their unique optical properties and shape-dependent plasmonic response. When resonantly excited, collective oscillations of the electron gas within these nanostructures can produce highly enhanced electromagnetic fields in their near-field zone. As a result, metallic NPs have great potential for several applications including subwavelength optical waveguiding, biosensing, surface-enhanced spectroscopy, and efficiency enhancement in solid-state light emitters and solar cells.^{1,2} The tunability of their optical properties is of particular importance from a practical standpoint. It is well known that varying the size and shape of individual metallic NPs allows for tuning of their localized surface plasmon resonance.^{3,4} Furthermore, electromagnetic interactions among NPs within arrays can also be used to spectrally shift these resonances by controlling particle spacing and array configuration.^{5–13} Such two-dimensional arrays can be chemically synthesized, as well as fabricated using a variety of lithographic techniques such as electron beam lithography (EBL), which provide an unprecedented degree of control for integration in a wide range of devices.

In typical studies of gold and silver NP arrays fabricated on planar substrates by lithographic techniques, plasmonic resonances at wavelengths from the 600 nm range into the near-infrared spectral region are reported.^{5–12} Shorter-wavelength resonances are also of great interest in several contexts, including for enhancing the efficiency of visible light-emitting devices. This application, which has attracted considerable attention in recent years,^{8,14–18} relies on the near-field excitation and subsequent scattering of surface plasmon polaritons in suitably designed metallic nanostructures. A large enhancement in light-emission efficiency (re-

lated to the average field intensity enhancement in the active layer) can correspondingly be obtained, provided that the emission wavelength is closely matched to the nanostructure plasmonic resonance. Metallic NP arrays with geometrically tunable resonances across the entire visible range are therefore critical to enable the widespread applicability of this approach. In fact, from a technological standpoint plasmon-enhanced light emission can be expected to be particularly important at green-yellow wavelengths in the 500–600 nm spectral region, which is currently lacking a suitable materials platform producing high-efficiency light-emitting devices.

In general, the plasmonic resonance wavelength of NP arrays can be blueshifted by reducing the particle diameter and/or by decreasing the interparticle spacing.^{3–13} However, practical limitations of current nanofabrication technologies, and the associated broadening due to size variations, limit the effectiveness of this approach. Furthermore, as the particle diameter is decreased optical absorption due to electron-phonon collisions within the metal begins to dominate over resonant light scattering.^{1,3} Therefore, exceedingly small NPs are not suitable to applications requiring efficient scattering of their plasmonic excitations, as in the case of plasmon-enhanced light emission. It should also be noted that the plasmonic resonance wavelength also depends on the NP composition, and can be blueshifted by using metals with larger plasma frequency such as aluminum.¹³ However, this approach is again generally accompanied by an increase in absorption losses compared with the use of silver and gold, due to the larger imaginary part of the dielectric function of aluminum at visible wavelengths.

In this work, we consider square arrays of Ag nanocylinders and investigate how their plasmonic properties can be tailored by controlling the NP height. In particular we show that the plasmonic resonance wavelength can be effectively blueshifted by increasing the particle height, while at the

^{a)}Electronic mail: rpaiella@bu.edu.

same time maximizing the average field enhancement in the substrate and maintaining small absorption losses. To that purpose, several NP arrays of different height and periodicity have been fabricated using EBL, characterized via transmission spectroscopy measurements, and numerically investigated using finite-difference time-domain (FDTD) simulations. The article is organized as follows. The experimental and numerical methods used in the fabrication, optical testing, and simulation of the NP arrays are described in Sec. II. In Sec. III we present the experimental and theoretical extinction spectra of the fabricated arrays from which the plasmonic resonance wavelength can be inferred and plotted versus NP height. The height dependence of the scattering versus absorption cross sections and of the associated electromagnetic field enhancement are also numerically investigated and discussed. The main conclusions of this study are then presented and summarized in Sec. IV.

II. EXPERIMENTAL AND SIMULATION METHODS

All the arrays studied in this work consist of Ag nanocylinders patterned on a planar sapphire substrate, arranged in a two-dimensional square lattice with overall dimensions of $60 \times 60 \mu\text{m}^2$. The NP diameter was kept fixed at 130 nm, large enough to ensure that the extinction cross section is generally dominated by scattering as opposed to absorption,^{1,3} and at the same time sufficiently small to avoid substantial radiation damping of the plasmonic oscillations.¹⁹ Several arrays were investigated with NP height ranging from 20 to 160 nm. Furthermore, since the height dependence of the array plasmonic response was found to vary with the NP center-to-center spacing (pitch), for each value of the height six different arrays were fabricated on the same substrate, with pitch ranging from 180 to 330 nm.

To fabricate each set of arrays, poly(methylmethacrylate) (PMMA) was first spun onto a sapphire substrate and patterned using a Zeiss scanning electron microscope (SEM) configured with an EBL nanometer pattern generation system. Following PMMA development, the sample was briefly descummed with a plasma asher under 200 (SCCM) (SCCM denotes standard cubic centimeters per minute at STP) of O_2 and 100 W of rf power. An Ag layer of the desired thickness was then deposited using an electron-beam evaporator, which was run at high vacuum ($\sim 2 \times 10^{-6}$ Torr) to produce smooth metallic films with small grain sizes. The Ag NPs were finally created via lift-off. Each step in the fabrication process was carefully characterized for optimal control of the NP geometry. The fabricated dimensions were verified by SEM imaging and atomic force microscopy. An exemplary SEM micrograph of an array with 270-nm-pitch is shown in Fig. 1. The relatively small variations in NP shape and diameter observed in this figure are representative of all fabricated samples. The system of coordinates used in the numerical simulations of the array plasmonic properties is also shown in this figure.

After fabrication, the array transmission spectra were measured by broadband illumination at normal incidence with unpolarized light from a deuterium tungsten halogen source. In these measurements, the samples were mounted

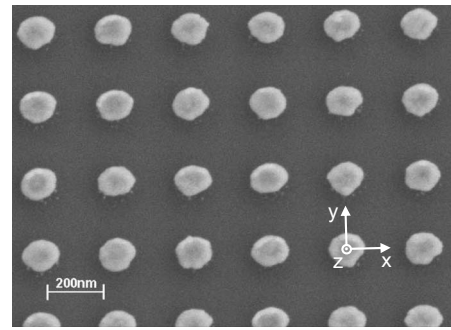


FIG. 1. SEM image of a two-dimensional square array consisting of cylindrical Ag NPs with 130-nm-diameter and 270-nm-pitch. Also shown is the system of coordinates used in the numerical simulations presented in this work.

on a piezocontrolled stage allowing submicron resolved translation, and two long-working-distance $20\times$ objectives were used to focus the incident light on each array and to collect the transmitted signal. The input objective was also used as part of a microscope allowing the individual arrays to be imaged for ease of alignment. The focused spot size was measured with the knife-edge method and found to be approximately $25 \mu\text{m}$. After transmission through each array, the collected signal was coupled into an optical fiber and finally analyzed with an Ocean Optics USB-4000 grating spectrometer. To isolate the extinction features due to the NP arrays only, all spectra were normalized to the transmittance of bare sapphire.

Numerical simulations were run for each pitch-height combination using a commercial FDTD package.²⁰ The dielectric functions of Ag (from Ref. 21) and sapphire were interpolated from known experimental data, and were further confirmed via separate ellipsometry measurements. All simulation parameters including mesh size, boundary conditions, excitation pulse length, and monitors positions were carefully selected and optimized. In each run, the computational window was defined so as to include exactly one repeat unit of the two-dimensional periodic array centered around a NP. The optimized computational mesh involved a refined region extending 10 nm beyond this NP in the x and y directions and 40 nm above and below the NP in the z direction. The mesh size in the x-y plane and along the z direction ranged from 3.5 and 1 nm, respectively, within the refined region to maximum values of 10 and 8 nm outside. Any further reduction in cell size was found to have no appreciable effect on the computational results. Periodic boundary conditions were employed in the plane of the particles (the x-y plane), while perfectly matched layers were used in the orthogonal (z) direction. The array scattering and absorption cross sections, steady-state field profiles, and field intensity enhancement factors were then calculated from field power monitors at different positions within the computational window. In the extinction spectra simulations, the NP arrays were illuminated at normal incidence with a broadband pulsed excitation having 2.65 fs pulse width, 565 nm center wavelength, and linear polarization along the x direction. To calculate the field profiles and enhancement factors, the center wavelength of the input pulses was then changed to the array resonance

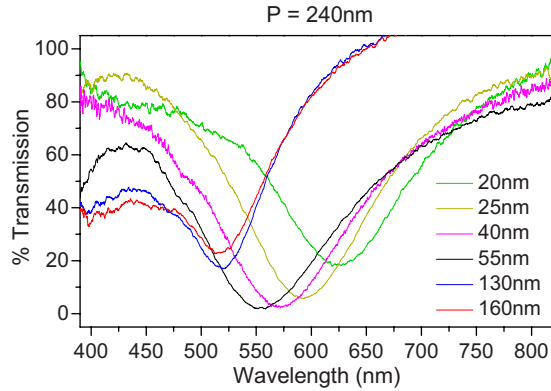


FIG. 2. (Color online) Measured transmission spectra of Ag NP arrays with 240-nm-pitch and varying NP height of 20, 25, 40, 55, 130, and 160 nm in order of decreasing wavelength of minimum transmission.

wavelength, as determined from the previously computed extinction spectra.

III. RESULTS AND DISCUSSION

The height dependence of the array plasmonic response is illustrated in Fig. 2, where we show the measured transmission spectra of six arrays with pitch $P=240$ nm and NP height H ranging from 20 to 160 nm. A pronounced resonance is seen in each spectrum, whose center wavelength strongly decreases with increasing height until it saturates for height values comparable to the NP diameter. The taller NPs also appear to exhibit an additional weaker transmission dip near the short-wavelength end of the accessible spectral range. The latter features are attributed to an asymmetric quadrupole (or double dipole) plasmonic excitation, as supported by the field-profile calculations discussed in the following. In Fig. 3 we show the main resonance wavelength (taken as the experimental wavelength of minimum transmission) plotted versus pitch for different NP heights. It is clearly seen that the resonance is spectrally blueshifted as the particle height increases for all array configurations, though the effect is more pronounced for arrays of smaller pitch. Furthermore, a blueshift is also generally observed with decreasing interparticle spacing, consistent with previous reports from similar nondiffracting NP arrays.^{5,6,9} Altogether the measured arrays cover a rather broad spectral range, extending to wavelengths below 500 nm, even though they all comprise relatively large (130-nm-diameter) NPs.

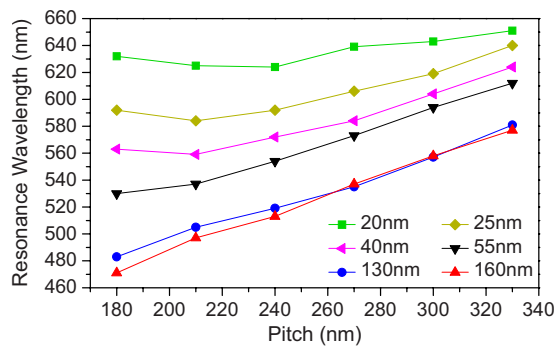


FIG. 3. (Color online) Measured plasmonic resonance wavelengths plotted vs array pitch for different NP heights (indicated in the legend).

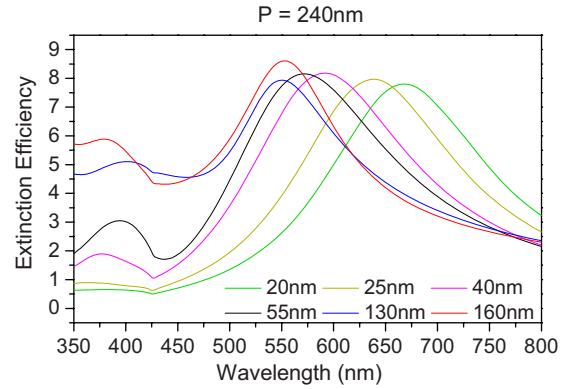


FIG. 4. (Color online) Calculated extinction efficiency spectra of Ag NPs in 240-nm-pitch arrays. The NP heights are 20, 25, 40, 55, 130, and 160 nm in order of decreasing wavelength of maximum extinction.

These experimental observations are well reproduced by our simulation results. To illustrate, in Fig. 4 we show a series of extinction efficiency spectra (defined as the ratio of the extinction cross section to the geometrical cross section) computed with the previously discussed method for the six arrays of Fig. 2. The same general behavior as in the experimental data is observed in this figure, including the appearance of a weaker shorter-wavelength resonance in the taller NP arrays. Incidentally, it should also be noted how the peak values of all these spectra are well above unity, which underscores the strength of the interaction between these Ag NPs and the incident light. The main resonance wavelength inferred from the simulated extinction spectra (i.e., the wavelength of peak extinction) is plotted versus array dimensions in Fig. 5, and exhibits the same trend of blueshifting with increasing NP height and decreasing pitch observed in Fig. 3. The overall quantitative agreement between theoretical and experimental values is also reasonably good, with larger discrepancies observed for smaller pitch and/or smaller height values and mainly attributed to fabrication size variations. In particular, SEM studies indicate variations in NP diameter within each array of up to about $\pm 5\%$ of the target value. Given the strong dependence of resonance wavelength on diameter, the vertical error in the experimental data of Fig. 3 can be mainly attributed to such fluctuations and estimated to be of similar magnitude. The resulting variations in NP spacing, as well as small uncertainties in the height, may also

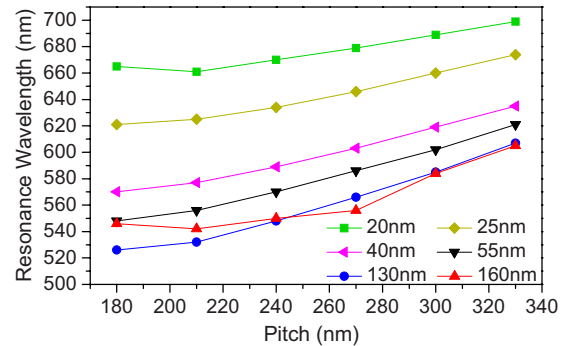


FIG. 5. (Color online) Calculated plasmonic resonance wavelengths plotted vs array pitch for different NP heights (indicated in the legend).

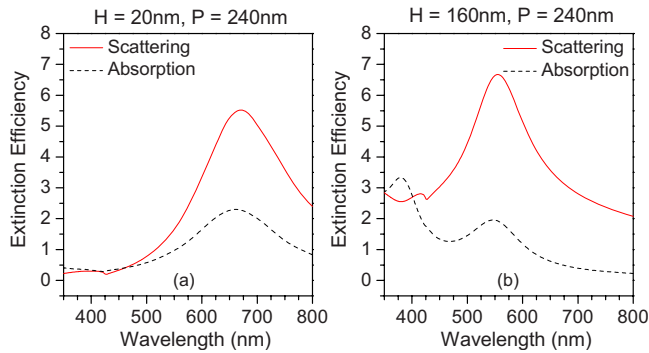


FIG. 6. (Color online) (a) Calculated scattering and absorption efficiency spectra of 20-nm-tall Ag NPs in a 240-nm-pitch array. (b) Same as in (a) for the case of 160-nm-tall NPs.

contribute to the observed discrepancies, particularly for the arrays with smaller pitch and/or smaller height values.

The observed height dependence of the array plasmonic response is consistent with the known variation of resonance wavelength with aspect ratio in nanoscale metallic ellipsoids, as discussed, e.g., in Ref. 3. A simple interpretation can also be constructed based on the harmonic oscillator model of localized plasmonic excitations, where the resonance frequency is proportional to the restoring force experienced by the displaced electrons on one side of the NP due to the background of exposed positive ions on the other side. As the NP size perpendicular to the displacement (the height in our case) is increased, the amount of charge induced on both sides by the incident optical field increases while their separation remains fixed. As a result, the displaced electron gas experiences a larger restoring force leading to a shorter resonance wavelength. Furthermore, the electromagnetic coupling among neighboring NPs in the array (which also causes a blueshift in resonance wavelength, as shown in Figs. 3 and 5) can be expected to be stronger for taller NPs. This can explain why the height dependence appears to be more pronounced in arrays of smaller pitch.

The results presented so far therefore show that the plasmonic resonance of lithographically defined NP arrays can be substantially blueshifted by increasing the NP height. From a practical standpoint, what is also important is that the resulting arrays still provide large scattering cross sections with minimal absorption and large electromagnetic field enhancements in their near-field zone. Both of these properties were therefore also investigated in our numerical simulations. Regarding the array extinction cross sections, the relative contributions due to scattering and absorption were calculated independently and compared. Typical results are shown in Figs. 6(a) and 6(b) for the case of an array with 240-nm-pitch and NP height of 20 and 160 nm, respectively. In both plots the scattering contribution is substantially larger than the absorption, at least in the spectral region of the main resonance. Furthermore, the scattering-to-absorption ratio is found to increase with increasing height, consistent with its general tendency to increase with increasing NP volume.^{1,3} Thus, the use of tall nanocylinders considered in this work allows blueshifting the plasmonic resonance while at the same time also improving the scattering efficiency.

To determine the field enhancement factors in the vicin-

ity of the NPs, the steady-state field intensity distributions under external illumination at resonance were first calculated. Exemplar results are shown in the log 10-scale maps of Fig. 7, where the electric field intensity is plotted versus position on the plane through the center of the simulated NP and parallel to the x and z axes (as defined in Fig. 1). As shown by these data, the field distributions are also strongly affected by the NP height. The case of short (20 nm) NPs is illustrated in Figs. 7(a) and 7(b), which correspond to arrays with 330- and 180-nm-pitch, respectively. In both figures, field distributions indicative of purely dipolar plasmonic excitations are observed. Furthermore, a comparison between these two plots suggests a decreased field penetration into the substrate (i.e., in the $z < 0$ space) as the particle separation is decreased. This behavior is attributed to the correspondingly increased interparticle coupling which tends to pull the optical field in the space between the NPs, as already discussed in Ref. 8.

More complex field distributions are obtained in the case of taller NPs, as illustrated in the remaining four panels of Fig. 7. Here the field distributions resemble the weighted superposition of two dipolar excitations, one centered near the NP upper corners and associated with the metal/air interface, the other centered near the lower corners and involving the metal/substrate interface.²² These two dipolar field distributions are clearly seen in Fig. 7(c), for the case of an array with 160 nm NP height and 330-nm-pitch excited at the center wavelength of its main extinction peak (605 nm). In this plot the metal/substrate dipolar field contribution appears to be more pronounced than the metal/air one. On the other hand, the opposite becomes true if the same array is excited at the center wavelength of its weaker, higher-frequency resonance (423 nm), as shown in Fig. 7(e). This behavior is consistent with the general nature of elementary dipolar excitations of metallic NPs, whose resonance wavelength increases with increasing dielectric constant of the surrounding medium.¹ Finally, in Figs. 7(d) and 7(f) we plot the field distributions of an array with the same large NP height (160 nm) but smaller pitch (180 nm), excited at its two resonance wavelengths. Similar double dipole modes can also be observed in this array, except that the optical field is now pulled more strongly in the space between the NPs, again due to the stronger interparticle coupling in arrays of smaller pitch.

Finally, the steady-state field intensity distribution of each NP array was integrated over a plane immediately beneath the particles (where a low-efficiency light-emitting layer may be located) and extending over the entire simulation window. This quantity was then divided by the intensity of the incident wave integrated over the same plane, resulting in an average field-intensity enhancement factor. The results of this analysis are illustrated in Fig. 8, where the average field-intensity enhancement factor is plotted versus NP height for different values of the array pitch. Specifically, the traces shown in Figs. 8(a) and 8(b) were computed on the plane at a distance of 5 and 20 nm below the NPs, respectively. Several observations can be made based on these data. First, relatively large values of the average enhancement factor (certainly suitable for applications such as light-emission

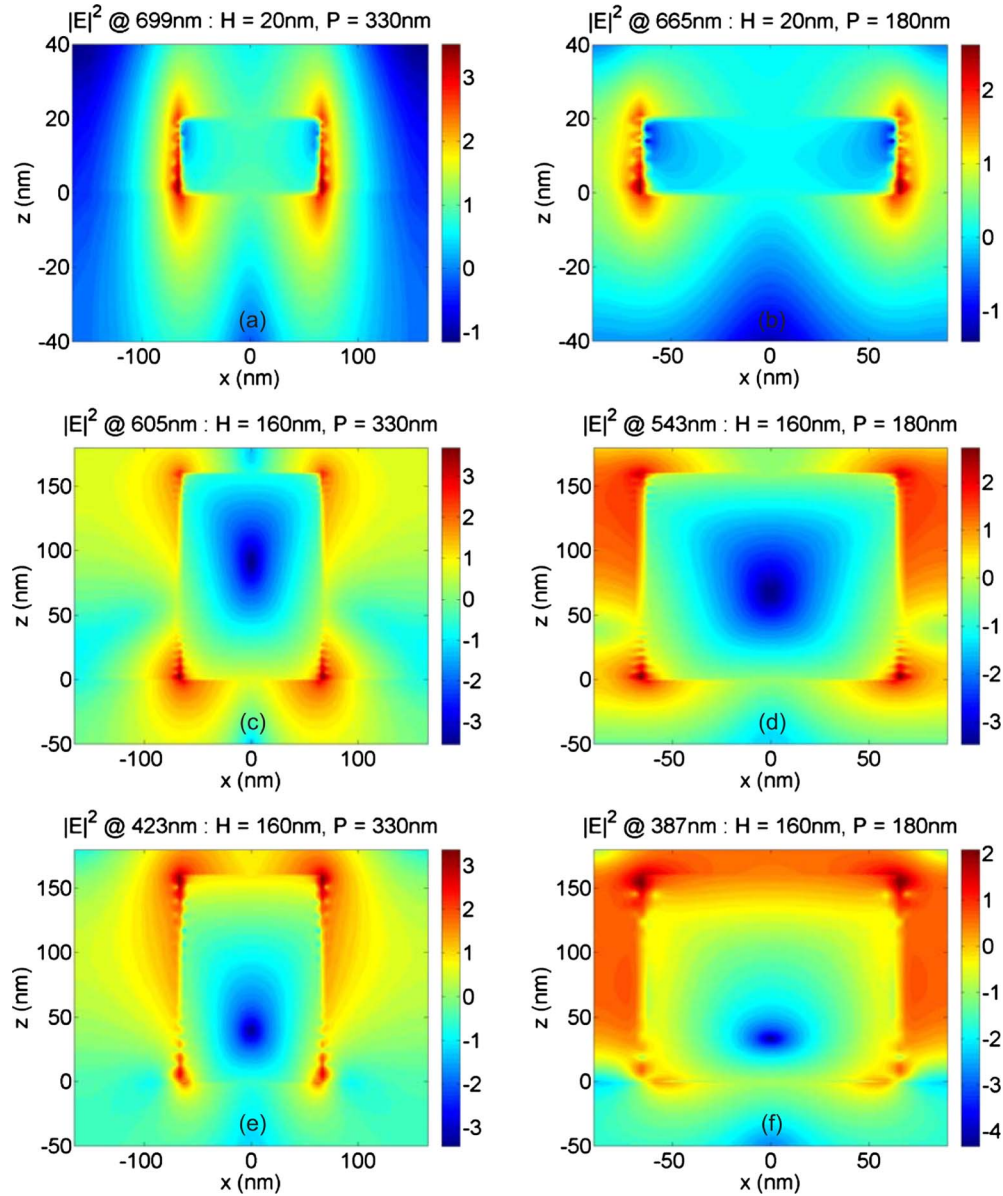


FIG. 7. (Color online) log 10-scale plots of the steady-state electric field intensity on the x - z plane through the center of the simulated NP for various arrays. The NP height H , the array pitch P , and the wavelength λ at which these field distributions were calculated are indicated in each panel. In panels [(a)–(d)], λ is the center wavelength of the main plasmonic resonance of the array under study. In panels [(e) and (f)], it coincides with the center wavelength of the weaker, higher-frequency resonance.

efficiency enhancement⁸) are generally obtained for the arrays under study. Second, the enhancement factor is found to decrease with decreasing pitch, which is due to the associated redistribution of the optical field in the space between the NPs.⁸ Third, the enhancement factor also rapidly decreases with increasing distance from the NPs [as in going from Fig. 8(a) to Fig. 8(b)], which is due to the well known evanescent nature of surface plasmon polaritons.

Finally, a more complex dependence involving an oscillatory behavior is observed versus NP height. This dependence can be explained by referring to the field-distribution plots of Fig. 7. As the NP height is increased, the field distribution initially evolves from that of a single dipolar excitation shown in Figs. 7(a) and 7(b) to the double dipole of Figs. 7(c)–7(f). At the height values where this transition takes place, the two field lobes on either side of each NP are

weakly confined in the plane of the array due to the limited available space, and therefore their penetration into the substrate below and vacuum above is particularly large. Correspondingly, the average enhancement factors of Fig. 8 go through a maximum near these values of NP height. A similar behavior is observed with even taller NPs, where a third dipole mode is found to appear in the field distribution (not shown) leading to a new maximum in enhancement factor, and so forth. Incidentally, it should also be noted that as the NP height is further and further increased, eventually the field enhancement can be expected to become limited by radiation damping.¹⁹ In any case, the results plotted in Fig. 8 clearly show that the short-resonance-wavelength arrays considered in this study can provide highly enhanced optical fields in their immediate vicinity, which again is a key prerequisite for many applications.

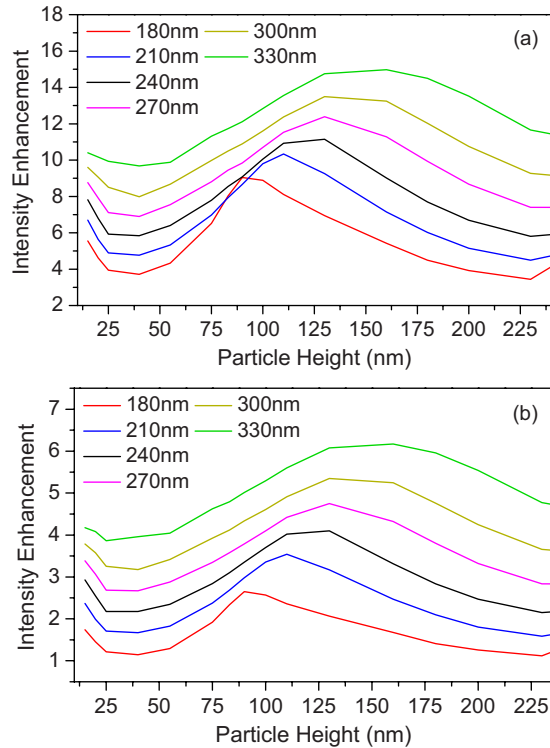


FIG. 8. (Color online) Average intensity enhancement factor on a plane at a distance of (a) 5 nm and (b) 20 nm below the NPs, plotted vs NP height for arrays of varying pitch (180, 210, 240, 270, 300, and 330 nm in order of increasing enhancement).

IV. CONCLUSIONS

In summary, we have presented a detailed experimental and theoretical study of the plasmonic properties of Ag NP arrays as a function of NP height. On the experimental side, several arrays have been fabricated by EBL and characterized via transmission spectroscopy measurements. The same arrays have also been numerically investigated via FDTD calculations of their extinction, scattering, and absorption cross sections and steady-state field intensity distributions. The measured transmission spectra feature pronounced extinction peaks whose center wavelengths strongly decrease with increasing NP height, in good agreement with the simulation results. The use of tall NP arrays therefore provides an effective way to blueshift the plasmonic resonance of lithographically defined metallic nanostructures. Additional FDTD calculations show that the same short-resonance-

wavelength NP arrays can also provide large scattering efficiencies and large field-intensity enhancements in the substrate. Specifically, the data plotted in Fig. 5 (or Fig. 3) and Fig. 8 can be used to maximize the latter parameter, while at the same time tuning the resonance wavelength over a wide range. These results are promising to extend the spectral reach of EBL-fabricated NP arrays for practical applications such as light-emission efficiency enhancement.

ACKNOWLEDGMENTS

This work was supported by the Department of Energy under Grant No. DE-FG02-06ER46332.

- ¹S. A. Maier, *Plasmonics: Fundamentals and Applications* (Springer, New York, 2007).
- ²*Surface Plasmon Nanophotonics*, edited by M. L. Brongersma and P. G. Kik (Springer, New York, 2007).
- ³C. F. Bohren and D. R. Huffman, *Absorption and Scattering of Light by Small Particles* (Wiley, New York, 1983).
- ⁴K. L. Kelly, E. Coronado, L. L. Zhao, and G. C. Schatz, *J. Phys. Chem. B* **107**, 668 (2003).
- ⁵B. Lamprecht, G. Schider, R. T. Lechner, H. Ditlbacher, J. R. Krenn, A. Leitner, and F. R. Aussenegg, *Phys. Rev. Lett.* **84**, 4721 (2000).
- ⁶C. L. Haynes, A. D. McFarland, L. L. Zhao, R. P. Van Duyne, G. C. Schatz, L. Gunnarsson, J. Prikulis, B. Kasemo, and M. Käll, *J. Phys. Chem. B* **107**, 7337 (2003).
- ⁷H. Mertens, J. Verhoeven, A. Polman, and F. D. Tichelaar, *Appl. Phys. Lett.* **85**, 1317 (2004).
- ⁸J. S. Biteen, L. A. Sweatlock, H. Mertens, N. S. Lewis, A. Polman, and H. A. Atwater, *J. Phys. Chem. C* **111**, 13372 (2007).
- ⁹J. Sung, E. M. Hicks, R. P. Van Duyne, and K. G. Spears, *J. Phys. Chem. C* **112**, 4091 (2008).
- ¹⁰B. Augu e and W. L. Barnes, *Phys. Rev. Lett.* **101**, 143902 (2008).
- ¹¹Y. Chu, E. Schonbrun, T. Yang, and K. B. Crozier, *Appl. Phys. Lett.* **93**, 181108 (2008).
- ¹²A. Ghoshal, I. Divliansky, and P. G. Kik, *Appl. Phys. Lett.* **94**, 171108 (2009).
- ¹³G. H. Chan, J. Zhao, G. C. Schatz, and R. P. Van Duyne, *J. Phys. Chem. C* **112**, 13958 (2008).
- ¹⁴W. L. Barnes, *J. Lightwave Technol.* **17**, 2170 (1999).
- ¹⁵K. Okamoto, I. Niki, A. Shvartser, Y. Narukawa, T. Mukai, and A. Scherer, *Nature Mater.* **3**, 601 (2004).
- ¹⁶R. Paiella, *Appl. Phys. Lett.* **87**, 111104 (2005).
- ¹⁷H. Mertens, A. F. Koenderink, and A. Polman, *Phys. Rev. B* **76**, 115123 (2007).
- ¹⁸G. Sun, J. B. Khurgin, and R. A. Soref, *J. Opt. Soc. Am. B* **25**, 1748 (2008).
- ¹⁹A. Wokaun, J. P. Gordon, and P. F. Liao, *Phys. Rev. Lett.* **48**, 957 (1982).
- ²⁰FDTD SOLUTIONS v. 6.0; Lumerical Solutions; Vancouver, British Columbia, Canada (2009).
- ²¹P. B. Johnson and R. W. Christy, *Phys. Rev. B* **6**, 4370 (1972).
- ²²C. H aggglund, M. Z ach, G. Petersson, and B. Kasemo, *Appl. Phys. Lett.* **92**, 053110 (2008).